Charge transfer energy and band filling effects on two-hole Auger resonances in strongly correlated systems

Prabhakar and Anamitra Mukherjee
School of Physical Sciences, National Institute of Science Education and Research, a CI of Homi Bhabha National Institute, Jatni 752050, India

(Received 26 May 2023; accepted 20 September 2023; published 3 October 2023)

We investigate the impact of charge transfer energy and band filling on the stability of the two-hole resonance relevant for Auger electron spectroscopy (AES) in transition-metal oxides. As a minimal model to study charge transfer effects in a transition metal (TM) and oxygen (OX) chain, we consider a one-dimensional chain with spinless fermions with an alternating motif of site-pairs with nearest-neighbor (NN) repulsion U and uncorrelated site-pairs, separated by a charge transfer gap Δ. We first show that while two holes added in a filled band of NN interacting fermions in one dimension can stabilize to a two-hole bound pair, the bound pair delocalizes with a U-dependent bandwidth. In contrast, we establish that the bandwidth of two holes added on a TM site pair in a filled band is dramatically suppressed, realizing a "local" two-hole resonance (L2HR) at the same TM site pair mimicking the AES phenomenology. Employing a memory-efficient exact numerical scheme and standard Lanczos-based diagonalization, we then study two-hole spectra for holes added at TM site pairs in partially filled bands. We analyze the multiple features that arise in the two-hole spectra at partial filling of the ground state. We uncover that in the strong-U limit, there is a filling-dependent Δ_{crit} above which the L2HR remains stable for any band filling greater than 75%. In this regime, the energy location of the L2HR provides a direct estimate of the correlation strength at TM site pairs for partial filling and is reminiscent of the Cini-Sawatzky theory for the filled band case. At 75% band filling, an abrupt redistribution of two-hole spectral weight destroys the L2HR regardless of the U or Δ values. We discuss the relevance of these nonperturbative results, obtained with full lattice symmetry, for understanding the AES of partially filled bands in terms of the local two-hole spectrum.

DOI: 10.1103/PhysRevB.108.165103

I. INTRODUCTION

Few-body bound states are of fundamental importance in the study of many-body physics. They lead to emergent properties that include superconductivity mediated by Cooper pairs, repulsively bound pairs in Bose-Hubbard models [1], trion bound states in GaAs quantum wells [2], Efimov states [3,4], and stable molecules. When these bound complexes are exact eigenstates, they represent true bound states. However, in many situations, the low-energy states are described by bound complexes interacting with a continuum of excitations, where the complexes acquire a finite lifetime and occur as resonances. Such resonances also occur in the study of two-hole bound complexes in the Auger electron spectroscopy (AES) of correlated materials [5–9].

The "core-valence-valence" or CVV Auger process consists of the decay of an x-ray-induced core hole into two final state valence holes plus an Auger electron and is mediated by on-site Coulomb interactions [9–11]. AES provides crucial insights into a local atomic multiplet structure, on-site interaction strengths, and crystal fields [12–14]. Further, supplementing AES of the transition element with oxygen KLL Auger spectra yields additional information on oxygen on-site repulsion energy and interactions between holes in neighboring transition-metal and oxygen ions [15]. Such information is vital for understanding correlated materials, making AES a longstanding focus of extensive research [16–24].

The well-known exact solution to the two-hole Green's function, the Cini-Sawatzky [10,11] theory, applies to simple cases, e.g., Cu, Zn where two holes are added in a full $3d$ band. In this case, the central quantity of interest, the local two-hole Green's function, can be computed from a non-interacting single-hole Green's function. The resulting local two-hole spectral function weighted with suitable matrix elements provides excellent agreement with experiments. Further generalizations to include dynamical screening, off-site interactions, overlap effects, and one-step formulation have helped sharpen the theoretical analysis [9,25]. However, in partially filled bands, success has been limited. The Green's function of two holes added at an atomic site in the background of holes in the partially filled ground state is a nontrivial many-body problem. Early attempts include ladder approximation [26–28] and diagrammatic vertex correction [29] approaches. They have achieved some success for partial filling close to the fully filled limit by adding a small number of holes in the filled band. Another standard approach to the problem is the impurity approximation. Here a transition-metal oxide with transition-metal (TM) ion intercalated with oxygen (OX) is simplified to an Anderson impurity problem of a single TM ion connected to an OX lattice [30–33]. More recently, variational approaches for computing few-body bound states in one dimension have been developed [34,35]. These approaches have added valuable insights to the two-hole propagator in partially filled bands. However, these methods have

shortcomings that need to be alleviated. Impurity models are computationally less intensive and can capture local atomic physics, but they lower the true lattice symmetries and do not exactly capture the effect of band filling. The many-body perturbative approaches are restricted to partial filling close to the filled ground state. Finally, the variational approach developed for the few-body Green's function is difficult to generalize to finite hole-doped ground states.

Here, we present numerically exact results of two-hole spectral functions for interacting spinless fermions in one dimension. These results go beyond perturbative approaches, retain full lattice symmetry unlike impurity approximations, and can be employed at any partially filled ground state. A repulsively two-hole bound state can be stabilized for spinless fermions with nearest-neighbor (NN) repulsion. Such a bound state delocalizes with a correlation-dependent bandwidth. The reason for considering spinless fermions is to limit the Hilbert space dimension to access larger system sizes. Since a single spinless fermion can occupy each site, the two-hole bound state comprises two holes on NN sites instead of being localized on a single site in actual AES. However, as discussed in the paper, the stability of the two-hole bound state is largely unaffected by the inclusion of spin degrees of freedom.

Another important experimental fact is that the two-hole bound state in AES remains localized near the atom where the core hole is created over experimental timescales. We consider a one-dimensional model with pairs of TM sites with NN interaction U separated by pairs of OX sites and add a charge transfer energy Δ between the TM and OX site pairs. We show that it is possible to drastically suppress the bandwidth of the two-hole bound state within our model, approximating an almost localized two-hole bound state. This "local" two-hole resonance within our model implies a pair of holes localized on a TM site pair. The nomenclature of TM and OX is borrowed from transition-metal and oxygen sites, respectively, in a transition-metal oxide chain. These energy scales are a natural first choice to investigate as, in transition-metal oxides, Coulomb interactions and charge transfer energy are dominant energy scales, for example, facilitating the well-known Zaanen-Sawatzky-Allen classification [36], and are also known to be the main driver of the two-hole resonance in AES [10,11]. Restricting to only these scales allows us to uncover how the ground-state charge fluctuation affects the Green's function of two holes added at a TM site pair over a wide range of hole-doped ground states. We investigate the model within an exact numerical scheme [37] and standard Lanczos-based diagonalization.

We first compute the two-hole spectral function in a filled ($n = 1$) lattice of spinless fermions with NN interaction U to set the stage. From this, we establish that two holes added on NN sites delocalize as a pair with a narrow U-dependent bandwidth, forming a two-hole bound pair beyond a critical U. We then consider a model that mimics the phenomenology of AES by creating a chain of uncorrelated OX site pairs and NN interacting TM site pairs with a correlation strength U and a charge transfer energy Δ between OX and TM. We show that unlike the simple NN repulsive model for $n = 1$, the two-hole bound pair is strongly localized (with vanishingly small bandwidth) at the TM site pair where they are initially added. However, its stability requires both large U and Δ. We refer to this resonance as a "*local*" two-hole resonance (L2HR), indicating two holes localized on a single TM site pair. We then investigate the interplay of Δ and band filling (n) in the strong interaction regime or for appropriately chosen large-U values.

We detail how partial filling ($n < 1$) of the ground state and Δ play out in the large-U limit by mapping out the $\Delta - n$ parameter regime where the L2HR is stable. We establish that the L2HR is stable for $0.75 < n \leqslant 1$, provided Δ is greater than a filling-dependent Δ_{crit}. By examining the detailed evolution of the two-hole spectral function with ground-state filling and Δ, we provide the reason for the observed limited range of stability in the $\Delta - n$ parameter space and the sudden redistribution of spectral weight at $n = 0.75$ that destroys the signature of the L2HR in the local two-hole spectral function. We show that in the regime where the L2HR is stable at partial band filling, its energy location varies linearly with U and Δ, similar to the Cini-Sawatzky theory for L2HR in filled bands. We conclude by commenting on the relevance of our results for Auger electron spectroscopy.

The paper is organized as follows. We summarize the theoretical approach for analyzing AES in Sec. II. Section III briefly discusses the many-fermion formalism for extracting the two-hole spectral function in real space. In Sec. IV A, we discuss the results of the NN interacting fermions. We discuss the results of the interplay of charge transfer, interaction, and doping on the stability of the L2HR for the TM and OX site-pair model in Sec. IV B. We conclude the paper in Sec. V.

II. GENERAL THEORY OF AUGER ELECTRON SPECTROSCOPY

We briefly discuss the theory of core-valence-valence (CVV) Auger scattering. The Auger scattering is a radiationless process in which an x-ray-induced core hole at an atomic site produces two valence band holes along with the emission of an Auger electron. Within the two-step model [10,11], the initial ionization of the atom by x ray and the Auger relaxation are treated independently. The initial state consists of a filled valence shell and an atomic site with a core hole. Assuming almost instantaneous thermalization of the core hole with its environment allows one to approximate the initial state energy E_i to be equal to $E_0^{\mathcal{N}} + E_c$. Here, E_c is the core-hole energy, and $E_0^{\mathcal{N}}$ is the ground-state energy of a Hamiltonian H_v describing the valence band electrons including kinetic energy and electron repulsion. In the Auger relaxation, a valence electron fills the initial core-hole state, and the energy that is released excites another valance band electron in a scattering state with energy $E_{\mathbf{k}}$. The sudden approximation allows one to treat the two-hole valence state and the emitted electron as independent processes. Thus, the final state energy can be identified with $E_f = E^{\mathcal{N}-2} + E_{\mathbf{k}}$, where $E_{\mathcal{N}-2}$ is the $(\mathcal{N}-2)$-electron excited state of the valance band Hamiltonian H_v.

The Auger transition is determined by the matrix element [38] $\int \varphi^*_{c\sigma}(\mathbf{R_I} - \mathbf{r_1})\varphi^*_{\mathbf{k}\sigma'}(\mathbf{r_2})|\frac{1}{|\mathbf{r_1}-\mathbf{r_2}|}|\varphi_{v\sigma'}(\mathbf{R_J} - \mathbf{r_1})\varphi_{v\sigma}(\mathbf{R_L} - \mathbf{r_2})d\mathbf{r_1}d\mathbf{r_2}$. The core-hole wave function at the atomic location $\mathbf{R_I}$ is denoted by $\varphi_{c\sigma}(\mathbf{R_I} - \mathbf{r_1})$ and a one-body scattering state for the Auger electron is $\varphi_{\mathbf{k}\sigma}(\mathbf{r_2})$. $\varphi_{v\sigma}(\mathbf{R_J} - \mathbf{r_1})$ and $\varphi_{v\sigma}(\mathbf{R_L} - \mathbf{r_2})$ denote the final state valence state wave

functions of two holes located at atoms at $\mathbf{R_J}$ and $\mathbf{R_L}$. Usually, the Auger process is dominated by intra-atomic contribution, allowing the simplification of identifying $\mathbf{R_I} = \mathbf{R_J} = \mathbf{R_K}$. We label this simplified matrix element by $M^{\sigma\sigma'}_{R_I}(\mathbf{k}) \equiv \frac{e^2}{4\pi\epsilon_0}\int \varphi^*_{c\sigma}(\mathbf{R_I}-\mathbf{r_1})\varphi^*_{\mathbf{k}\sigma'}(\mathbf{r_2})|\frac{1}{|\mathbf{r_1}-\mathbf{r_2}|}|\varphi_{v\sigma'}(\mathbf{R_I}-\mathbf{r_1})\varphi_{v\sigma}(\mathbf{R_I}-\mathbf{r_2})d\mathbf{r_1}d\mathbf{r_2}$. In terms of the Fermi golden rule, we have the momentum-resolved Auger intensity proportional to $|M^{\sigma\sigma'}_{R_I}(\mathbf{k})|^2\delta(E^{\mathcal{N}-2}+E_\mathbf{k}-E_0^{\mathcal{N}}-E_c)$. Defining $(E_\mathbf{k}-E_c)\equiv\hbar\omega$, we have $\mathcal{I}_{R_I}(\omega,\mathbf{k}) = \sum_{\sigma,\sigma'}|M^{\sigma\sigma'}_{R_I}(\mathbf{k})|^2\delta(\hbar\omega+E^{\mathcal{N}-2}-E_0^{\mathcal{N}})$. The δ function contains information on the $(\mathcal{N}-2)$-fermion excitations in the $\mathcal{N}$-fermion ground state of H_v, generated by two electrons removed from the site $\mathbf{R_I}$. This local two-hole spectral function can be obtained from the Fourier transform of the corresponding local two-hole Green's function with two holes created simultaneously in the $\mathcal{N}$-fermion ground state of the atom at $\mathbf{R_I}$ and subsequently removed together. Thus, from a many-body perspective, the central quantity of interest is the two-hole local propagator with two-time labels.

For a one-orbital lattice Hamiltonian describing a valence band with spin-full fermions and on-site repulsion (Hubbard model), the Green's function to be computed would involve two holes of opposite spins added at the site $\mathbf{R_I}$. In the present study, as discussed in Sec. I, we consider spinless fermions with nearest-neighbor interactions in a one-orbital lattice model. Here, the double occupation of a single site is Pauli blocked. Thus, in our model with interacting spinless fermions, *two-hole localization refers to holes localized on adjacent lattice sites*. Thus, the relevant Green's function to be computed involves two holes on adjacent sites, as elaborated in the next section.

III. METHOD

We consider a periodic lattice of $\mathcal{L}$ sites with $\mathcal{N}$ fermions. Based on the discussion in the previous section, our quantity of interest is the retarded two-hole propagator $G^{(2h)}_{IJ;IJ}(t,t') \equiv \langle\psi_0^{\mathcal{N}}|c_I^\dagger(t')c_J^\dagger(t')c_I(t)c_J(t)|\psi_0^{\mathcal{N}}\rangle$, where two fermions are destroyed at sites I and J at a time t, and added back at the same site pair at a later time t', in the many-fermion ground state $|\psi_0^{\mathcal{N}}\rangle$ with ground-state energy $E_0^{\mathcal{N}}$. The real-space two-hole spectral function in the frequency space $A^{(2h)}_{IJ;IJ}(\omega)$ is given by $-1/\pi\,\mathrm{Im}\{G^{(2h)}_{IJ;IJ}(\omega)\}$, where $G^{(2h)}_{IJ;IJ}(\omega)$ is the Fourier transform of $G^{(2h)}_{IJ;IJ}(t,t')$.

For an interacting Hamiltonian H defined on a $\mathcal{L}$ site periodic chain with $\mathcal{N}$ fermions, we consider a generic eigenvalue problem $\hat{H}|\lambda^{\mathcal{N}}\rangle = E_\lambda^{\mathcal{N}}|\lambda^{\mathcal{N}}\rangle$, where $\{E_\lambda^{\mathcal{N}}\}$ and $\{|\lambda^{\mathcal{N}}\rangle\}$ are the $\mathcal{N}$-particle eigenvalues and eigenvectors, respectively. We have employed atomic units that amount to setting $\hbar$, electron charge (e), electron mass m_e, and $1/4\pi\epsilon_0$ equal to 1. We choose a real-space $\mathcal{N}$-fermion basis $\{|j_\mathcal{N}\rangle\} \equiv \{c^\dagger_{a_1}\ldots c^\dagger_{a_\mathcal{N}}|0\rangle\}$, whose elements are generated by permuting real-space fermion positions, here denoted by the a_i subscripts of the creation operators.

We emphasize that the real-space basis is constructed from the fermion occupations of lattice sites in real space, more appropriately called the site basis. In the compact $\{|j_\mathcal{N}\rangle\}$ basis notation, the $\mathcal{N}$-fermion Green's function is denoted by $\mathcal{G}^{\mathcal{N}}_{i_\mathcal{N};j_\mathcal{N}}(\omega)$. We note that the $\mathcal{N}$-fermion Green's function is a matrix $[\mathcal{G}^{\mathcal{N}}(\omega)]$ in the $\{|j_\mathcal{N}\rangle\}$ basis and defines the $\mathcal{N}$-fermion spectral function matrix by the relation $[\mathcal{D}^{\mathcal{N}}(\omega)] \equiv -1/\pi\{\mathrm{Im}[\mathcal{G}^{\mathcal{N}}(\omega)]\}$. A trace of the $\mathcal{N}$-fermion spectral function matrix $[\mathcal{D}^{\mathcal{N}}(\omega)]$ taken over the $\mathcal{N}$-fermion basis provides the $\mathcal{N}$-fermion density of states $\mathcal{A}^{\mathcal{N}}(\omega)$.

For two holes created at site pair (I,J) in the many-fermion ground state $|\psi_0^{\mathcal{N}}\rangle$ and subsequently destroyed from the same locations, the real-space two-hole spectral function is given by

$$A^{(2h)}_{IJ;IJ}(\omega) = \sum_{j_\mathcal{N},j'_\mathcal{N}} \mathcal{D}^{\mathcal{N}}_{j_\mathcal{N},j'_\mathcal{N}}\left(E_0^{\mathcal{N}}\right)\mathcal{D}^{\mathcal{N}-2}_{j_\mathcal{N}(IJ)^-;j'_\mathcal{N}(IJ)^-}(\omega). \quad (1)$$

The details of the derivation are standard and are provided in Sec. 1 of the Appendix. From the formula, we see that the two-hole spectral function is expressed in terms of elements of the $\mathcal{N}$- and $(\mathcal{N}-2)$-fermion spectral function $[\mathcal{D}^{\mathcal{N}}(\omega)]$ and $[\mathcal{D}^{\mathcal{N}-2}(\omega)]$, respectively. The relation $|j_\mathcal{N}(IJ)^-\rangle = c_I c_J|j_\mathcal{N}\rangle$ defines the indices of $[\mathcal{D}^{\mathcal{N}-2}(\omega)]$ in Eq. (1). The definitions for the primed labels are analogous. The elements of $[\mathcal{D}^{\mathcal{N}}(\omega)]$ are needed at $\omega = E_0^{\mathcal{N}}$, the $\mathcal{N}$-fermion ground-state energy. $E_0^{\mathcal{N}}$ is determined from the lowest-energy peak of the $\mathcal{N}$-fermion density of states, $\mathcal{A}^{\mathcal{N}}(\omega)$. Different elements of $\mathcal{D}^{\mathcal{N}}_{j_\mathcal{N},j'_\mathcal{N}}(E_0^{\mathcal{N}})$ are extracted from the $\mathcal{N}$-fermion Green's function $\mathcal{G}^{\mathcal{N}}_{j_\mathcal{N};j'_\mathcal{N}}(\omega) = \langle j_\mathcal{N}|\hat{\mathcal{G}}(\omega)|j'_\mathcal{N}\rangle$, evaluated between the $\mathcal{N}$ particle basis elements, $(|j_\mathcal{N}\rangle)^\dagger$ and $|j'_\mathcal{N}\rangle$. We calculate $[\mathcal{G}^{\mathcal{N}}(\omega)]$, $[\mathcal{G}^{\mathcal{N}\pm1}(\omega)]$ and $[\mathcal{G}^{\mathcal{N}-2}(\omega)]$ using a recently developed memory-efficient variant of full exact diagonalization. The scheme is outlined in Sec. 2 of the Appendix; we refer the reader to our recent work for details and numerical benchmarks [37].

IV. RESULTS

A. Repulsive spinless fermions in 1D

We first study the spectral response of a filled ($\mathcal{L}=\mathcal{N}$) or $n=1$ many-body ground state to the introduction (and subsequent removal) of two holes in the spinless-fermion model with NN repulsion. We define the model with periodic boundary condition (pbc) on a $\mathcal{L}$ site chain with NN interactions, as follows:

$$H = -t\sum_{\langle I,J\rangle}(c_I^\dagger c_J + \mathrm{H.c.}) + U\sum_I n_I n_{I+1}, \quad (2)$$

where $c_I^\dagger$ (c_I) are spinless fermion creation (annihilation) operators at the site I. t and U are the NN hopping and interaction, respectively. $n_I = c_I^\dagger c_I$ is the number operator at a site I. We measure all energies in units of t, which we have set to unity. We analyze the properties of two holes created in a filled system ground state by calculating the *total* two-hole spectral function, $\sum_{I\neq J}A^{(2-\mathrm{hole})}_{IJ;IJ}(\omega) \equiv A^{(2-\mathrm{hole})}(\omega)$. We also calculate the *local* two-hole spectral function $A^{(2-\mathrm{hole})}_{IJ;IJ}(\omega) \equiv A^{(2-\mathrm{hole})}_L(\omega)$ for holes created on NN sites I and J. In the present case, the term "local" implies the spectral function for holes on NN sites, the closest analog of on-site in the spin-full problem.

Figure 1(a) shows $A^{(2-\mathrm{hole})}(\omega)$ for different values of U where the spectrum is shifted by the ground-state energy $E_0^{\mathcal{N}}(=\mathcal{N}U)$. For $U=0$, we have the two-hole continua

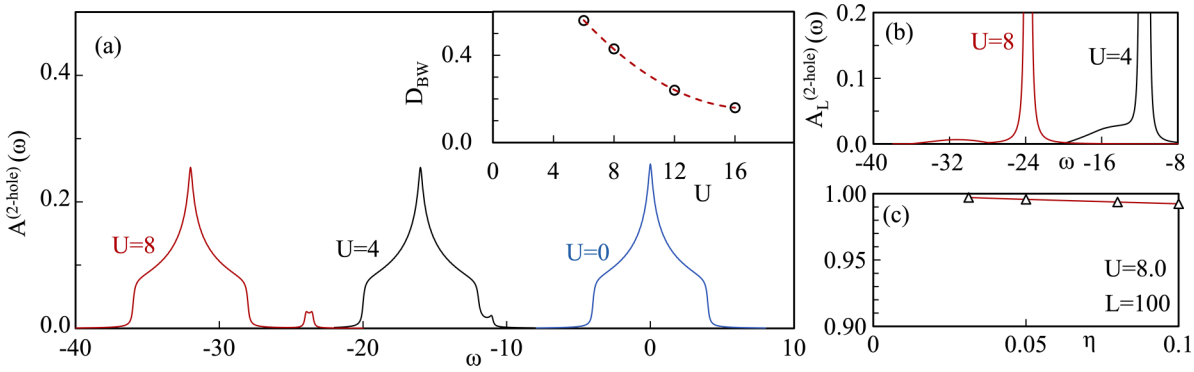

FIG. 1. Two-hole excitation spectrum in a filled ground state for spinless fermions with NN interacting. (a) The two-hole spectral function $A^{(2-\text{hole})}(\omega)$ for indicated U values. The dissociation of the single continua into two distinct features is shown for $U = 8$. The inset in (a) shows the comparison of the numerical bandwidth of the two holes delocalizing as a bound pair (circles) and analytic scaling (dashed line). (b) The local two-hole spectral function $A_L^{(2-\text{hole})}(\omega)$ for $U = 4$ and 8. (c) The ratio of the numerical and exact frequency two-hole spectral sum rule value as a function of broadening factor η. All results are for a $\mathcal{L} = 100$ site chain with periodic boundary conditions.

extending from $\omega \approx -4t$ to $\omega \approx 4t$. This feature is the two-hole band comprised of the holes moving independently, respecting the Pauli exclusion principle, and agrees with the analytical form $\sum_{k\neq k'} \delta[\omega + 2t\cos(k) + 2t\cos(k')]$, with the k (k') sums extending over the entire Brillouin zone $[-\pi, \pi)$. For $U = 4$, we see that the band center is at $\omega \approx -16$ or $4U$ below zero. We also see that the two-hole spectral function is distorted compared to the $U = 0$ case, and a small feature appears at the upper band edge. Beyond $U = 5$, this feature splits off, creating a band with two holes delocalizing as a pair. We show typical data for $U = 8$, where we find a band of width 8, centered around $\omega = -32$, and a narrow band centered at $\omega = -24$. To understand the spectrum, we analyze the *potential energy of the basis states*. The potential energy is the correlation energy of the fermion configurations in a basis state in the limit of no hopping. For all basis states containing the two holes on nearest-neighbor sites, the potential energy is $(\mathcal{N} - 3)U$, while for all other two-hole basis states, it is $(\mathcal{N} - 4)U$. Since we shifted the spectra by the ground-state energy ($\mathcal{N}U$), the centroids of the two bands with states containing two holes not on nearest-neighbor sites are at $-4U$. Similarly, the states with two holes on NN sites contribute to the band centered around $-3U$. The finite bandwidths result from kinetic energy that gives a width of $8t$ for the two holes delocalizing independently and a much smaller bandwidth to the other band. The inset in Fig. 1(a) shows the scaling of the bandwidth of the narrow band (D_{BW}) as a function of U by open symbols. The solid lines are the results from an analytical projection approach that agrees well with the numerical results. Details of the analytical calculation are presented in Sec. 3 of the Appendix.

To further clarify the character of the split off-peak, in Fig. 1(b), we show $A_L^{(2-\text{hole})}(\omega)$ for holes created (and subsequently destroyed) on a pair of adjacent sites I and J. For $U = 4$, we find a wide distribution of spectral weight over the entire width of the total two-hole spectral function. Significant overlap exists between the sharp peak near -10 and the broad continua. In contrast, for $U = 8$, we see a clear split-off feature at $U = -24$ and well-separated, bandlike continua coinciding with the two-hole band centered around -32 in Fig. 1(a). The split-off feature has the same width as D_{BW} [inset in Fig. 1(a)], showing that the two holes delocalize as a pair. However, it has a small overlap with the broad band centered at -32, implying that this feature is a signature of a two-hole *bound pair* and has a finite lifetime.Similar repulsively bound states have been reported for bosons with $U \gg t$ [1,39] and the spin-full Hubbard model within Density Matrix Renormalization Group (DMRG) [40].

We would like to briefly discuss the numerical accuracy of these results. As is well known, from the analytic properties of the Green's function, by shifting the poles of the Green's function above and below by a regulator η, the real axis defines the retarded and advanced Green's function. The expression for the retarded Green's function with a finite η is provided in Eq. (A1). Thus, our two-hole spectral function derived from the Green's function depends on η. A standard way to understand the systematics of η dependence of the two-hole spectral function is to compute the two-hole frequency sum rule for different values of η and compare the result with the theoretical value of $\mathcal{L}(\mathcal{L} - 1)$. Hence, in Fig. 1(c), we show the two-hole frequency sum rule plot as a function of η. It is defined as $\int_{-\infty}^{\infty} A^{(2-\text{hole})}(\omega)d\omega$, whose exact analytical value is $\mathcal{L}(\mathcal{L} - 1)$, for two holes in a filled band. The ratio of the numerical value to $\mathcal{L}(\mathcal{L} - 1)$ rapidly approaches 1, as $\eta \to 0$.

Before we move on to the main model investigated in our paper, we comment on the essential difference between the spin-full fermion and the present study with spinless fermions. We emphasize that the main question being addressed in this paper is the validity of the local two-hole spectral function as a signature of Auger spectroscopy in partially hole-doped bands. Spin physics is not expected to play a dominant role in determining the critical parameter values of the location of the split-off feature. For example, the location of the split-off feature in the main panel of Fig. 2(b) is given by $-2\Delta - U$. This closely agrees with previous work with two-body spin-full fermions' split-off feature in [34].

B. Interplay of band filling and charge transfer energy

We now consider the impact of band filling and charge transfer effects in the presence of strong interactions on the

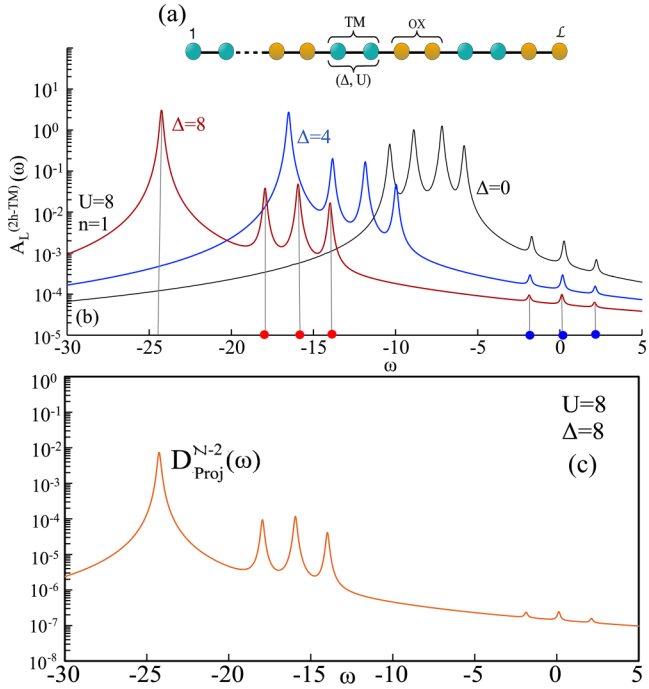

FIG. 2. *Local* two-hole spectral function at TM site pair in filled bands. (a) Schematic of the periodic model. (b) The local two-hole spectral function for a pair of holes created on a TM site pair for $n = 1$ and three Δ values, as indicated. Results shown are for $U = 8$ and $\mathcal{L} = 100$. The vertical lines for $\Delta = 8$ mark the locations of the centers of the three features. The red and blue ellipses on the ω axis are discussed in the text. (c) Projected $\mathcal{D}^{\mathcal{N}-2}_{\rm Proj}(\omega)$ which quantifies the contribution to the $(\mathcal{N}-2)$-fermion spectral function from basis states with two holes doubly occupying any TM site pair.

local two-hole spectral function. The model is defined as follows:

$$H = -t\sum_{\langle I,J\rangle}(c_I^\dagger c_J + \text{H.c.}) + U\sum_{I=1}^{\mathcal{L}/4} n^{\rm TM}_{4I-3}n^{\rm TM}_{4I-2} + \Delta\sum_{I=1}^{\mathcal{L}/4}\left(n^{\rm TM}_{4I-3}+n^{\rm TM}_{4I-2}\right). \quad (3)$$

In Fig. 2(a), we show a schematic of the Hamiltonian. The chain contains pairs of sites labeled as TM sites with on-site energy ($\Delta \geqslant 0$) and nearest-neighbor (NN) repulsion strength of U among them. The TM site pairs are separated by pairs of sites labeled as OX sites with $U = 0$. Δ acts as a charge transfer energy between the TM and OX sites. Thus the TM site pair with NN interactions acts as the simplest extension of an alternating chain of TM and OX with spin-full fermions. The spinless-fermion model allows us to examine the formation of two spatially localized holes on adjacent lattice sites as opposed to on-site localization in the spin-full fermion case. Below we show that indeed, such two-hole resonances are stabilized in certain situations. We refer to such two-hole resonances as "local" two-hole resonance (L2HR). As pointed out at the end of the previous section, the locations of the two-hole spectral function features remain largely unaffected by spin excitations. Further, inclusion of spins severely restricts the lattice sizes that can be accessed due to significantly enlarged Hilbert space. For these reasons, we choose to work with the spinless-fermion model.

The creation (annihilation) operators have the usual meaning. I, J in the kinetic energy term runs over NN sites. $n_I^{\rm TM}$ is the number of operators on the TM site I. The OX sites are noninteracting sites. We also define $n_I^{\rm OX}$ as the number of operators on the OX site I. With these identifications, we define $n = \frac{1}{\mathcal{L}}(\sum_I n_I^{\rm TM} + \sum_I n_I^{\rm OX})$, where the sum runs over TM and OX sites in the first and second summations, respectively. Here, $\mathcal{L}$ refers to the total number of sites. In terms of these, we define fully filled ($n = 1$) and partially filled ($n < 1$) bands. This $n = 1$ refers to a system where all TM and OX sites are fully occupied. Finally, the hopping between all sites is t.We study local two-hole spectra for two holes created on adjacent TM sites in the filled ($n = 1$) and partially filled [$(n < 1)$ or $(1 - n)$] hole-doped ground states on $\mathcal{L}$ sites with pbc. For the present model, the local two-hole spectral function of interest is for two holes created on a single TM site pair, as mentioned above. These TM holes hybridize with holes states in OX sites and can delocalize through the system.

(i) Local two-hole spectrum in the undoped case. In Fig. 2(b), we show the local two-hole spectral function defined as $A^{(2-\text{hole})}_{IJ;IJ}(\omega) \equiv A_L^{(2h-TM)}(\omega)$, where I and J are adjacent sites belonging to a TM site pair. The result is shown for $U = 8$ and three values of Δ for a 100-site lattice. The results are presented in a logarithmic scale on the y axis to clearly show the various structures. The ground-state energy for the fully filled case is $E_0^{\mathcal{N}} = \mathcal{L}(U + 2\Delta)/4$, as U and Δ are present only for the TM sites. As above, all the results are shifted by $E_0^{\mathcal{N}}$. For $\Delta = 8$, we see a well-separated feature at $\omega = -2\Delta - U(= -24)$. This energy corresponds to the potential energy reduction at $t = 0$ measured from the ground-state potential energy. It is identical for all basis states, with the two holes doubly occupying a TM site pair. The next structure is centered around $\omega = -\Delta - U(= -16)$, the potential energy of basis states with one hole on the TM site and one in the OX sites. Finally, the highest-energy feature centered around $\omega = 0$ refers to the case where both holes are on OX sites. We notice that the second and third features, respectively, are two and five orders of magnitude smaller than the first feature. To go beyond the simple potential energy-based analysis, we note that for the filled case, $\mathcal{D}^{\mathcal{N}}_{j_{\mathcal{N}},j'_{\mathcal{N}}}(E_0^{\mathcal{N}}) = 1$ as there is only one state, i.e., the filled many-body configuration. This is because $D^{\mathcal{N}}_{j_{\mathcal{N}},j_{\mathcal{N}}}(E_0^{\mathcal{N}}) = \mathcal{A}^{\mathcal{N}}(E_0^{\mathcal{N}}) = 1$, which is simply the $\mathcal{N}$-fermion spectral function evaluated at the ground-state energy. Thus, from Eq. (1), we see that the $A^{(2-\text{hole})}_{IJ;IJ}(\omega) = \sum_{j_{\mathcal{N}},j'_{\mathcal{N}}}\mathcal{D}^{\mathcal{N}-2}_{j_{\mathcal{N}}(IJ)^-;j'_{\mathcal{N}}(IJ)^-}(\omega)$. To ascertain that the peak at $-2\Delta - U = -24$ in Fig. 2(b) for $U = \Delta = 8$ is indeed a two-hole local resonance, we compare the $A_L^{(2h-TM)}(\omega)$ with $\mathcal{D}^{\mathcal{N}-2}_{\rm Proj}(\omega) = \sum_{\mathbf{j}_{\mathcal{N}-2}}\mathcal{D}^{\mathcal{N}-2}_{\mathbf{j}_{\mathcal{N}-2};\mathbf{j}_{\mathcal{N}-2}}(\omega)$, where the $\mathbf{j}_{\mathcal{N}-2}$ label runs only over the basis states which have the two holes together on any TM site pair for $U = \Delta = 8$. Figure 2(c) shows the projected spectral function. We immediately see that the peak of this quantity coincides with that of $A_L^{(2h-TM)}(\omega)$. Since $A_L^{(2h-TM)}(\omega)$ only contains the TM site-pair projected contribution, it clearly shows that the peak at $-2\Delta - U$ is indeed the local two-hole resonance. Moreover, the trace over the projected basis also shows that the effective bandwidth of

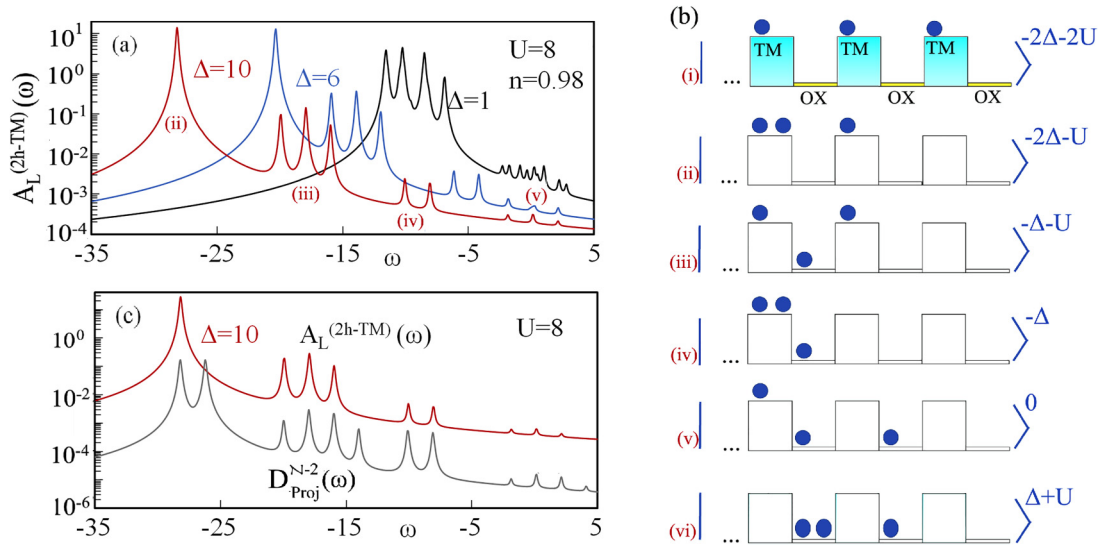

FIG. 3. *Local* two-hole spectral function in the almost filled ground state or at small hole doping. (a) The local two-hole spectral function for a pair of holes created on a TM site pair. The results are for doping values $n = 0.98$, $U = 8$, and three Δ values. (b) The six possible three-hole configurations in increasing order of their potential energies (from top to bottom). The TM site pairs are shown as a single level, elevated by Δ from the OX site pairs, as labeled in the top configuration. Filled circles denote the holes in an otherwise filled system. The potential energies for each configuration are indicated as superscripts for every state. The schematic only shows representative configurations in every case. (c) Comparison of the two-hole spectra (red) and projected three-hole spectral function contribution (gray). The projection involved in the gray curve is discussed in the text.

the two holes delocalizing only over only the TM pairs is negligible. The effective Hamiltonian approach, as was discussed for the NN interaction model in the previous section, also provides an infinitesimally small bandwidth in the present case.

The almost vanishing bandwidth (within numerical accuracy) leads to the strong spatial localization of $A_L^{(2h-TM)}(\omega)$ at the TM site pair where the two holes were created and stabilizes the *local* 2-hole resonance (L2HR). This preference of the *local* two-hole resonance also suppresses the other possible feature centered around $-2\Delta - 2U$, corresponding to both holes occupying different TM sites, to negligibly small values.

Reducing Δ to 4, we see a clear shift of spectral weight from the two-hole resonance primarily to the central feature. The three features are still centered around $-2\Delta - U$, $-\Delta - U$, and zero. However, we notice that the relative height of the central feature also grows roughly by one order of magnitude. As for $\Delta = 8$, the $\mathcal{D}_{\rm Proj}^{\mathcal{N}-2}(\omega)$ projected onto the basis states of two holes on a TM site pair still has the dominant contribution at the peak at $-2\Delta - U$, allowing the interpretation of this feature as the L2HR.

Finally, for $\Delta = 0$, the resonance merges with the central feature (centered at $-U$) and the L2HR is lost. On the other hand, if $U = 0$ and Δ is nonzero, the potential energies of the basis states that contribute to $-2\Delta - U$ and $-2\Delta - 2U$ become degenerate, the ground state has comparable contributions from the two holes of TM site pairs, and they are singly occupying different TM site pairs. Hence we conclude that a combination of U and Δ is needed to stabilize a well-separated resonance, primarily localized on the TM site pair in the undoped case. For completeness, we briefly discuss the origin of the substructures centered around $\omega = -16$ and $\omega = 0$ seen in Fig. 2(b) for $U = 8$ and $\Delta = 8$. The basis-state potential energy for one TM hole and one OX hole is $-\Delta - U = -16$, and is zero for both holes on OX. Since the states with two holes on TM hybridize with the above two categories of states, they show features around the locations $\omega = -16$ and $\omega = 0$. The support of the features on the ω axis is controlled by the spread of the spectrum belonging to the states of the two categories. Of course, the magnitudes are highly suppressed because of large Δ and U. The red (blue) ellipses on the ω axis in Fig. 2(b) show the eigenvalues of the Hamiltonian diagonalized in the restricted basis containing one TM and one OX hole (two OX holes). We find that these locations agree with the substructures around $\omega = -16$ and $\omega = 0$. We note that due to large U and Δ, the effect of hybridization which would shift the locations of these substructures (usual level repulsion effects) is small. They are likely to be more relevant at smaller U and Δ values.

(ii) Local two-hole spectrum for small doping. In Fig. 3(a), we show $A_L^{(2h-TM)}(\omega)$ for a ground state of $\mathcal{N} = 47$ fermions in a $\mathcal{L} = 48$ site lattice. The resulting filling, $n \sim 0.98$, is the smallest nontrivial doping possible at this system size, consisting of a single hole in the $\mathcal{N}$-fermion ground state. For the partially filled case, we first work out $\mathrm{Tr}\{\mathcal{D}^{\mathcal{N}}_{j_{\mathcal{N}}, j_{\mathcal{N}}}(\omega)\}$ and locate the lowest-energy peak, which gives the $\mathcal{N}$-fermion ground-state energy for the given Hamiltonian. As before, we shift $A_L^{(2h-TM)}(\omega)$ by the ground-state energy. We see in Fig. 3(a) that the two-hole spectrum develops more features than the filled case due to additional charge fluctuations since one hole is already present in the ground state. To analyze $A_L^{(2h-TM)}(\omega)$, shown in Fig. 3(a), we first list all the possible three-hole configurations once we create two extra

holes. Figure 3(b) shows the six possible kinds of three-hole configurations in order of increasing energy from (i) to (vi). Superscripts for each configuration denote their potential energies as measured from the lowest possible potential energy of the basis states. The "lowest possible potential energy" corresponds to the potential energy of the $\mathcal{N}$-fermion basis state with the ground-state hole on any TM site pair. All basis states belong to one of the six groups; depending on the total occupation of the TM and OX sites, the schematic shows some representative conjugations of each group.

For $\Delta = 10$, we see four dominant structures centered around $\omega = -2\Delta - U(= -28)$, $\omega = -\Delta - U(= -18)$, $\omega = -\Delta(= -10)$, and $\omega = 0$. These correspond to the configurations (ii)–(v) in Fig. 3(b). The lowest-energy configuration shown in Fig. 3(b) is $-2\Delta - 2U$. This feature is strongly penalized, as discussed for the undoped case.

Further, in Fig. 3(a), we find that with reducing Δ, the initially suppressed features gain in magnitude, the centroid of the feature (ii) rapidly approaches (iii), and, for $\Delta \leqslant 2$, it merges with the other structures. For example, for $\Delta = 6$, the features (ii)–(iv) move close to each other. There is also an overall shift of all the low-energy features toward zero. Finally, for $\Delta = 1$, we see that the features (ii)–(iv) merge.

We now analyze $A_L^{(2h-TM)}(\omega)$ with $n = 0.98$ for $\Delta = 10$ based on the many-fermion density of states. From Eq. (1), we crucially observe that the ω dependence of $A_L^{(2h-TM)}(\omega)$ comes *only from* $(\mathcal{N}-2)$*-fermion density of states (DOS)*. In Fig. 3(c), we show $\mathcal{D}^{\mathcal{N}-2}_{\rm Proj}(\omega) = \sum_{\mathbf{j}_{\mathcal{N}-2}} \mathcal{D}^{\mathcal{N}-2}_{\mathbf{j}_{\mathcal{N}-2},\mathbf{j}_{\mathcal{N}-2}}(\omega)$ in gray, where, the $\mathbf{j}_{\mathcal{N}-2}$ label now runs only over the basis states where two holes are on any pair of TM sites and the third hole is on any other TM pair. We choose to project into these basis states since the $\mathcal{N}$-fermion ground state is dominantly made up of the basis states where the ground-state hole occupies TM rather than OX.

To compare, we replot in Fig. 3(c) (red curve) the corresponding $A_L^{(2h-TM)}(\omega)$ for $\Delta = 10$, from Fig. 3(a). Unlike in the undoped case where $D^{\mathcal{N}}_{j_{\mathcal{N}},j_{\mathcal{N}}}(E_0^{\mathcal{N}}) = 1$, here we see that even in the presence of a single hole in the ground state, the $D^{\mathcal{N}}_{j_{\mathcal{N}},j'_{\mathcal{N}}}(E_0^{\mathcal{N}})$ has a significant effect. In particular, only the low-energy peak of $\mathcal{D}^{\mathcal{N}-2}_{\rm Proj}(\omega)$ at $(\omega = -2\Delta - U = -28)$ corresponding to configuration (ii) of Fig. 3(b) retains its contribution in $A_L^{(2h-TM)}(\omega)$. Similar reduced contributions are seen for all other features as well. This suppression of the features results from the summation over $j_{\mathcal{N}}$ and $j'_{\mathcal{N}}$ and the fact that the off-diagonal elements of the $\mathcal{N}$ and $\mathcal{N}-2$ particle spectral function matrices are not positive definite. We have also explicitly performed restricted summation over the $j_{\mathcal{N}}$ and $j'_{\mathcal{N}}$ in Eq. (1), such that only one of the six possible $(\mathcal{N}-2)$-fermion basis-state groups contribute at a time to $\mathcal{D}^{\mathcal{N}-2}(\omega)$. From this analysis, we have ascertained that apart from the basis states where two holes occupy a single TM site pair and the third hole is on any other TM pair, no other basis state has an appreciable contribution to the two-hole spectrum at $\omega = -2\Delta - U$. A similar analysis for other basis-state groups shows highly suppressed contributions to the peak at $-2\Delta - U$ for $\Delta = 10$ and $\Delta = 6$. For $\Delta = 1$, many of the six basis-state groups contribute at all energies, wiping out the signature of the L2HR from the local two-hole spectral function.

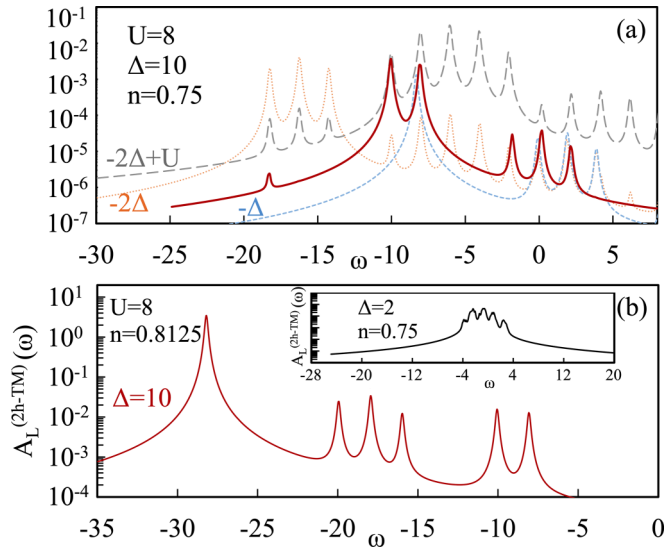

FIG. 4. *Local* two-hole spectral function in large hole-doped ground states. (a) The local two-hole spectral function for pair of holes created on adjacent TM sites for $n = 0.75$, for $\Delta = 10$ and $U = 8$, by the solid line. The dotted (orange), dashed (gray), and thin-dashed (blue) lines show the $(\mathcal{N}-2)$-fermion spectral function projected on basis states with potential energies -2Δ, $-2\Delta + U$, and $-\Delta$, respectively. (b) The two-hole spectral function for $n = 0.8$, which has four holes in the ground state compared to five at $n = 0.75$ for $\mathcal{L} = 20$, the size studied here. The inset in (b) shows the two-hole spectral function for $n = 0.75$ and small $\Delta(= 2)$.

(iii) Larger hole-doping case. We now consider $n = 0.75$ or 25% hole doping in the ground state. For reducing computational cost, we limit the computation to $\mathcal{L} = 20$ and $\mathcal{N} = 15$ or five holes in the ground state. In Fig. 4(a), we show $A_L^{(2h-TM)}(\omega)$ for $\Delta = 10$ and $U(= 8)$ by the solid red curve.

We also show the $(\mathcal{N}-2)$-fermion spectral function projected onto three sets of $(\mathcal{N}-2)$-fermion basis states with the lowest three potential energies. These three curves depict $\mathcal{D}^{\mathcal{N}-2}_{\rm Proj}(\omega)$, projected onto the basis states with potential energies -2Δ, $-2\Delta + U$, and $-\Delta$, measured from the lowest possible basis-state potential energy. These correspond to basis-state groups with only two, three, and one TM site pair doubly occupied by holes, respectively. Comparing the peak locations of $A_L^{(2h-TM)}(\omega)$ with the three $(\mathcal{N}-2)$-fermion projected spectral function, we find that the lowest peak in $A_L^{(2h-TM)}(\omega)$ has contributions from basis states with potential energies -2Δ, followed by those with potential energy $-2\Delta + U$. From the above, these basis states have two and three TM site pairs doubly occupied by holes. The most prominent peak in $A_L^{(2h-TM)}(\omega)$ has a contribution from basis states with three TM site pairs doubly occupied by holes and from basis states with two TM site pairs doubly occupied by holes. In fact, the $(\mathcal{N}-2)$-fermion basis states that have only one TM pair doubly occupied by holes and well separated from other features are those with potential energy $-\Delta$ (blue thin-dashed line) and contribute to the third features of $A_L^{(2h-TM)}(\omega)$. We have explicitly checked that among the 17 possible $(\mathcal{N}-2)$-fermion basis-state groups with distinct potential energies, no other groups contribute to the low-energy

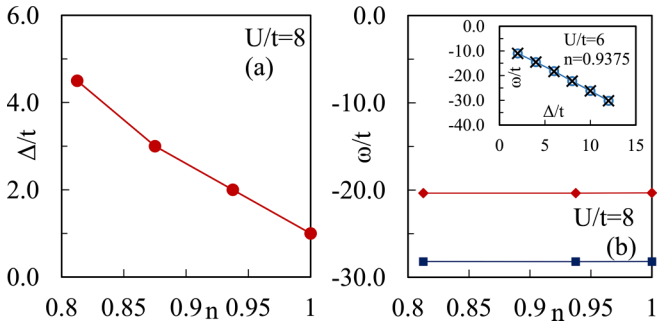

FIG. 5. Doping dependence of $\Delta_{\rm crit}$ for local two-hole resonance. (a) Δ-filling (n) plot showing the critical charge transfer energy for well-defined local two-hole resonance for large $U(=8t)$. (b) The scaling of the energy location of the L2HR feature with Δ for $\Delta > \Delta_{\rm crit}$. The main plot shows the hole-doping dependence of the L2HR peak location (centroid) for $\Delta = 6t$ (diamonds) and $8t$ (squares) for fixed $U(=8t)$. The inset shows the L2HR centroid locations with varying $\Delta > \Delta_{\rm crit}$ for $U = 6t$ at $n = 0.9375$ with open symbols. The crosses are obtained from Lanczos.

peaks of $A_L^{(2h-TM)}(\omega)$. Thus, the lowest-energy peak can no longer be interpreted as L2HR. In contrast, in Fig. 4(b), we show $A_L^{(2h-TM)}(\omega)$ for $n = 0.8$ for the same system size, Δ and U. This case has only one less hole in the $\mathcal{N}$-fermion ground state or four holes compared to five for $n = 0.75$. We see that $A_L^{(2h-TM)}(\omega)$ for $n = 0.8$ has a clear low-energy feature, whose composition is similar to the low-doping cases discussed earlier and can be interpreted as L2HR. We do not repeat the analysis here. This rather drastic spectral weight redistribution with a small change in hole doping can be rationalized in the following manner.

The two-hole addition on a TM site pair is only possible on basis states with at least one TM site pair doubly occupied by two fermions. At $n \leqslant 0.75$, the ground state is dominantly composed of basis states where all fermions reside on OX at large Δ and U. The basis states where two-hole addition only has finite amplitude have to have at least one doubly occupied TM site pair. However, these $\mathcal{N}$-fermion basis states have higher potential energies compared to those where the TM is singly occupied or unoccupied and, consequently, have small contributions to the ground-state wave function. For completeness, in the inset of Fig. 4(b), we show $A_L^{(2h-TM)}(\omega)$ for small $\Delta(=2)$, which, as expected, does not have any clear resonance peak. In summary, at $n = 0.75$, the spectral weight of the two-hole spectral function is strongly distributed among features constructed out of basis states where holes doubly occupy multiple TM site pairs. We note that these conclusions hold for larger system sizes as well. Regardless of the system size for $n \leqslant 0.75$, there are basis states where no TM site pairs are doubly occupied with fermions. Since the ground state for large U and Δ is dominantly constructed out of such basis states, the matrix element for creating two holes on a TM site pair is significantly suppressed.

(iv) Critical Δ for local two-hole resonance. Figure 5(a) shows the plot of the critical Δ needed for a well-defined L2HR as a function of hole doping of the ground state. The critical Δ is defined to the Δ value for which a single low-energy resonance (centered at $-2\Delta - U$) is pulled out of the rest of the two-hole spectral function features. The U is set to be larger than the kinetic energy bandwidth, as is typical for $3d$ TM oxides. We also consider positive Δ, which, apart from small bandwidth dependent corrections, dictates that holes doped to create a partially filled ground state prefer to occupy the TM site pairs, similar to doped Mott insulators. In the regime of Δ where we have a stable L2HR, we numerically observe this to be true. Also, a similar $\Delta < 0$ analysis can be carried out, mimicking a negative-charge transfer situation. However, in partially filled bands, if added holes prefer OX, the matrix element for creating two holes on TM is very small. We thus only consider positive Δ. At zero hole doping, the $\Delta_{\rm crit}/t \sim 1$ and increases linearly with hole doping, up to about slightly less than 75% band filling. Beyond that, as discussed for $n \leqslant 0.75$ above, there is a drastic redistribution of spectral weight in the local two-hole spectral function, destabilizing the L2HR for any Δ, while for $n > 0.75$, two-hole resonance can be stabilized for $\Delta > \Delta_{\rm crit}$.

(v) Relevance for L2HR in AES. As Sec. I mentions, the core-valence-valence AES, a core hole, decays into two final state holes in the valence band and an Auger electron. If the interaction between two final state holes is weak, the holes delocalize over the lattice screened from each other, with the AES or the two-hole spectral function closely resembling the convolution of two holes. In this case, the AES signal is proportional to the two-hole convolution. In the strongly correlated limit, the strong interaction can localize the electrons at the atomic site where they were created, shifting the energy higher than the screened two-hole energy by the Coulomb correlation. This fact is central to the Cini-Sawatzky theory for analyzing the AES experiments. They calculated the two-hole local Green's function for holes added to a filled d band exactly in terms of the one-hole Green's function. The approach shows that a split-off resonance with d^8 multiplet structure is generated whose energy location is U_{dd}, from the energy where two holes are on different sites or the band part of the spectrum. This theory captures the experimental spectra for filled $3d$ band systems such as Cu and Zn quite well. However, the major drawback of the theory is that the exact result holds when the one-hole Green's functions are known. For example, even for Ni, which is $3d^8$, the one-hole Green's function added in a partially filled $3d$ band is nontrivial and direct input for x-ray photoelectron spectroscopy (XPS) is needed [41].

As in the Cini-Sawatzky theory, impurity calculations [30] in the filled limit shows a satellite peak separated from the bandlike features by the local correlation strength. In this limit, the impurity results also show a simple linear relation of the satellite's location with U. However, adding small-hole doping before the Auger two-hole insertion strongly distorts the picture, even when core-hole effects are not considered. The linear dependence of the satellite peak is lost and the satellite shifts towards the bandlike part with increasing U. Finally, the effects of Δ have not been systematically explored at partial filling within the impurity studies to the best of our knowledge.

From Fig. 5(a), we already see that the L2HR, or the AES satellite, is stable beyond a filling-dependent $\Delta_{\rm crit}$. We briefly comment on the Δ dependence of the energy location of L2HR at large U. In the inset in Fig. 5(b), we see that for

hole doping of less than 25%, ($n > 0.75$), the L2HR location exhibits a simple linear dependence of $-U - 2\Delta$ for large fixed $U(= 6)$ for $n < 1$. This is representative of the behavior for all $n > 0.75$ and Δ greater than the n-dependent critical value. This is analogous to the linear dependence on U in the literature previously reported in the undoped case [30]. However, unlike the impurity approach, retaining the full lattice symmetry extends the regime where the L2HR has a linear dependence on U above 75% band filling.

Since Δ can be determined from x-ray techniques such as XPS [42], U can be ascertained for the location of the L2HR. Figure 5(b) shows the *filling independence* of the energy location of the L2HR for $0.75 < n \leqslant 1$. Representative data are shown for $U = 6$ and $U = 8$. We finally note that all results presented here using the low-memory approach are benchmarked against Lanczos-based diagonalization. As an example, in the inset in Fig. 5(b), we show that the Lanczos-based L2HR peak (crosses) is in excellent agreement with our method.

We conclude this section with general remarks summarizing the interplay of Δ and U, expectations in two dimensions, and spin-full cases. For two spinless holes added in a filled ground state of our one-dimensional model, we first consider the noninteracting problem, including nonzero Δ. When U crosses the minimum magnitude of the noninteracting two-hole band, a spectral feature is split from the noninteracting continuum. However, the split-off feature contains contributions from states with two holes on a single TM site pair, one hole each on TM and OX, both holes on OX, and both individually occupying two different site pairs. These features are centered around $-2\Delta - U$ and $-\Delta - U$, 0, and $-2\Delta - 2U$, as discussed earlier. Thus, to separate the L2HR centered around $-2\Delta - U$ from the other features, Δ has to be suitably chosen. The separation between these features depends on the feature centroids and the bandwidth of individual features. Thus, we have employed large U in our paper so that Δ can be chosen to isolate the L2HR.

With this understanding, we can consider the two-dimensional extension of our spinless fermion model with 2×2 plaquettes of TM and OX. Since the two-hole bandwidth is larger in two dimensions, the critical U (for a fixed Δ) to create split-off features is expected to be larger than in one dimension. Similarly, since the individual features will have more delocalization paths in two dimensions, their bandwidths are expected to be larger. Thus, for the same fixed large U in one and two dimensions, the Δ_{crit} needed to separate the L2HR is expected to be greater in two dimensions. The same trend should also hold for two holes added in partially filled ground states. Moreover, due to the 2×2 plaquette structure, the two-hole spectral function is expected to have a substructure even if two holes are spatially localized on a single plaquette. Thus, the occupation of a TM plaquette by two holes will reduce the energy from the filled ground state by $-4U - 2\Delta$ for holes occupying diagonal sites of the plaquette, followed by $-3U - 2\Delta$ when the two holes occupy adjacent sites on a TM plaquette. For one hole on OX, the energy reduction is $-2U - \Delta$, and 0 for both holes on OX. A careful analysis would be needed to determine the critical Δ at large U beyond the above general expectations, for the feature centroids.

The most straightforward material realistic extension of the model can be done by considering the well-known ionic Hubbard model [43,44] with a spin-full fermion in two dimensions. The model consists of TM and OX sites (to use the language in the paper) and can be studied in the case with on-site Hubbard U and Δ on TM sites (which can be occupied by two electrons of opposite spins) and noninteracting OX sites with zero on-site potential. The model is of relevance to strongly correlated double perovskites [45]. The U_{crit} for two holes added in a filled band will be approximately $U \geqslant \sqrt{\Delta^2 + 64t^2}$, twice the noninteracting one-hole bandwidth. U set to be much larger than this critical value will allow adjusting Δ to separate an on-site TM local two-hole resonance.

V. CONCLUSIONS

We have investigated the impact of strong correlation and charge transfer effects on the stability of a local two-hole spectral function in partially filled ground states using exact numerical techniques retaining full lattice symmetry. We have established that in contrast to only NN repulsive interaction, in the model with the TM and OX motif, both interaction and charge transfer energy are necessary for stabilizing a two-hole resonance with vanishing small bandwidth even in a filled ground state. For strong correlations, we have uncovered a charge transfer regime where the L2HR is stable for a wide regime of partially filled ground states, from filled to about 75% filling. At 75% band filling, the local two-hole spectral function shows an abrupt and dramatic spectral weight redistribution, destabilizing the signature of the L2HR in the local two-hole spectral function. For $n \leqslant 0.75$, the L2HR cannot be recovered for any U and Δ, unlike for $n > 0.75$. Finally, we have shown that the location of the L2HR has a linear relation of both Δ and U, for $\Delta > \Delta_{\text{crit}}$. In this regime, one could use the energy location of the L2HR to extract the value of TM interaction strength, which is an extension of the Cini-Sawatzky-type approach for ascertaining correlation strength from L2HR to partial band filling. Further, since our result produces the exact two-hole spectral function, the approach provides a way to fit the relevant experimental data in any parameter regime. Our numerical scheme can also handle the inclusion of core holes and can handle local multiplet structures and, in the future, will allow us to make a realistic comparison with AES experiments.

ACKNOWLEDGMENTS

All computations were preformed in the NOETHER, VIRGO and KALINGA high performance clusters at NISER. We acknowledge funding from the Department of Atomic Energy, India under Project No. 12-R&D-NIS-5.00-0100. A.M. would also like to acknowledge the SERB-MATRICS grant (Grant No. MTR/2022/000636) from the Science and Engineering Research Board (SERB) for funding.

APPENDIX

1. Many-fermion formalism

For two holes created on a pair of lattice sites (I, J) in a $\mathcal{N}$-fermion ground state $|\psi_0^{\mathcal{N}}\rangle$ and subsequently destroyed

at a later time from the same site pair, the two-hole retarded Green's function, in the frequency domain, is given by

$$G^{(2h)}_{IJ;IJ}(\omega) = \sum_{j_{\mathcal{N}}, j'_{\mathcal{N}}} \langle \psi_0^{\mathcal{N}} | j_{\mathcal{N}} \rangle \langle j'_{\mathcal{N}} | \psi_0^{\mathcal{N}} \rangle \times \langle j_{\mathcal{N}} | c_I^\dagger c_J^\dagger [(\omega + i\eta)I - H]^{-1} c_I c_J | j'_{\mathcal{N}} \rangle . \tag{A1}$$

In the above, we have inserted a complete set of $\mathcal{N}$-fermion real-space basis sets $\{|j_{\mathcal{N}}\rangle\}$ and $\{|j'_{\mathcal{N}}\rangle\}$. The two-hole spectral function is obtained from the imaginary part of the above expression. We first provide a way to obtain the prefactors $\langle \psi_0^{\mathcal{N}} | \, | j_{\mathcal{N}} \rangle \, \langle j'_{\mathcal{N}} | \, | \psi_0^{\mathcal{N}} \rangle$ and extract the factors in Eq. (A1) from the $\mathcal{N}$-fermion Green's function introduced in Sec. III. For this, we note that from the imaginary part of the $\mathcal{N}$ fermion, the Green's function in the Lehmann representation can be expressed as

$$-\frac{1}{\pi}\mathrm{Im}\mathcal{G}^{\mathcal{N}}{}_{j_{\mathcal{N}};j'_{\mathcal{N}}}(\omega) = \sum_{\lambda^{\mathcal{N}}} \langle j_{\mathcal{N}} | \, | \lambda^{\mathcal{N}} \rangle \, \langle \lambda^{\mathcal{N}} | \, | j'_{\mathcal{N}} \rangle \delta\big(\omega - E^{\mathcal{N}}_{\lambda}\big), \tag{A2}$$

which implies that

$$-\frac{1}{\pi}\mathrm{Im}\mathcal{G}^{\mathcal{N}}{}_{j_{\mathcal{N}};j'_{\mathcal{N}}}\big(\omega = E_0^{\mathcal{N}}\big) = \langle j_{\mathcal{N}} | \, | \psi_0^{\mathcal{N}} \rangle \langle \psi_0^{\mathcal{N}} | \, | j'_{\mathcal{N}} \rangle = D^{\mathcal{N}}_{j_{\mathcal{N}};j'_{\mathcal{N}}}\big(E_0^{\mathcal{N}}\big) \tag{A3}$$

in the $\eta \to 0$ limit, where $D^{\mathcal{N}}_{j_{\mathcal{N}};j'_{\mathcal{N}}}(\omega)$ is the $\mathcal{N}$-fermion spectral function matrix. We note that the above holds for $\mathcal{G}^{\mathcal{N}}_{j_{\mathcal{N}};j'_{\mathcal{N}}}(\omega) = \mathcal{G}^{\mathcal{N}}_{j'_{\mathcal{N}};j_{\mathcal{N}}}(\omega)$, which is true for equilibrium many-fermion problems. The remaining part of Eq. (A1) is matrix elements of the $(\mathcal{N}-2)$-fermion spectral function matrix $[\mathcal{D}^{\mathcal{N}-2}(\omega)]$. Thus, the two-hole real-space spectral function, $A^{(2h)}_{IJ;IJ}(\omega) \equiv -1/\pi \, \mathrm{Im}\{G^{(2h)}_{IJ;IJ}(\omega)\}$, can be expressed as

$$A^{(2h)}_{IJ;IJ}(\omega) = \sum_{j_{\mathcal{N}}, j'_{\mathcal{N}}} \mathcal{D}^{\mathcal{N}}_{j_{\mathcal{N}}, j'_{\mathcal{N}}}\big(E_0^{\mathcal{N}}\big) \mathcal{D}^{\mathcal{N}-2}_{j_{\mathcal{N}}(IJ)^-;j'_{\mathcal{N}}(IJ)^-}(\omega). \tag{A4}$$

While this form is true for any site pair (I, J), we particularly focus on the case when I and J are the NN of each other. In this case, we refer to the two-hole spectral function as a *local* two-hole spectral function, $A^{2-hole}_{IJ;IJ}(\omega) \equiv A^{2-hole}_{L}(\omega)$. From Eq. (A4), we first notice that the calculation of real-space two-hole spectral function $A^{(2h)}_{L}(\omega)$ involves elements of the $\mathcal{N}$-fermion spectral function matrix $\mathcal{D}^{\mathcal{N}}_{j_{\mathcal{N}}, j'_{\mathcal{N}}}(\omega)$, evaluated at $\omega = E_0^{\mathcal{N}}$ or at the many-fermion ground-state energy. Different elements of $\mathcal{D}^{\mathcal{N}}_{j_{\mathcal{N}}, j'_{\mathcal{N}}}(\omega)$ are extracted from the many-fermion Green's function $\mathcal{G}^{R(\mathcal{N})}_{j_{\mathcal{N}};j'_{\mathcal{N}}}(\omega) = \langle j_{\mathcal{N}} | \hat{\mathcal{G}}(\omega) | j'_{\mathcal{N}} \rangle$, evaluated between the $\mathcal{N}$-fermion basis elements, $(|j_{\mathcal{N}}\rangle)^\dagger$ and $|j'_{\mathcal{N}}\rangle$, at $\omega = E_0^{\mathcal{N}}$. The $(\mathcal{N}-2)$-fermion spectral function matrix elements required in Eq. (A4) are similarly extracted from $[\mathcal{G}^{\mathcal{N}-2}(\omega)]$. The $j_{\mathcal{N}}, j'_{\mathcal{N}}$ indices run over all the $\mathcal{N}$-fermion basis states, while the relation $|j'_{\mathcal{N}}(IJ)^-\rangle \equiv c_I c_J |j'_{\mathcal{N}}\rangle$ defines the $(\mathcal{N}-2)$-fermion basis indices in Eq. (A4). The unprimed indices refer to the corresponding conjugate states and are defined analogously.

Finally, we note that two-particle excitations in partially filled bands can be computed from $\mathcal{N}$- and $(\mathcal{N}+2)$-fermion spectral function matrices. Similarly, one (particle/hole) photoemission excitation can be computed from $\mathcal{N}$- and $(\mathcal{N}+1/\mathcal{N}-1)$-fermion spectral function matrices.

2. Fock-space recursive Green's function scheme

Here we briefly discuss the Fock-space recursive Green's function (F-RGF) scheme [37]. We have a $\mathcal{L}$ site chain with periodic boundary conditions containing $\mathcal{N}$ spinless fermions. We divide the lattice into two halves and label all $\mathcal{N}$-fermion states by $|n_l, n_r\rangle$. Here, n_l (n_r) refers to the number of fermions in the left (right) half. Under nearest-neighbor hopping, either (n_l, n_r) is conserved, implying no hopping between the two halves or a change only by ± 1 if the fermions hop between the two halves. Thus, the $\mathcal{N}$-fermion Hilbert space can be decomposed into a direct sum of $(\mathcal{N}+1)$ "Fock-space sectors" with fixed (n_l, n_r) and hopping matrices connecting them. The latter connects $|n_l, n_r\rangle$ to $|n_l \pm 1, n_r \mp 1\rangle$. We label the Fock-space sector with (n_l, n_r) occupations by α_{n_l+1}. The Hamiltonian for a particular Fock-space sector α_i is denoted by $H(\alpha_i)$, which contains $n_l = i-1$ and $n_r = \mathcal{N} - n_l$ in the left and right halves. The hopping matrices that connect nearest-neighbor sectors α_i and α_j are denoted by $[\tau]_{\alpha_i,\alpha_j}$. Since the connections are NN, the Hamiltonian has a tridiagonal representation in the Fock-space sector representation. Due to this, the inverse of the resolvent operator, $\omega + i\eta - H$, is also tridiagonal.

The main task is to obtain the resolvent operator or the $\mathcal{N}$-fermion Green's function. We will exploit the tridiagonal form of H and the inverse resolvent $\omega + i\eta - H$ for the inversion. The tridiagonal representation with NN Fock-space sector coupling matrices and sector Hamiltonians is similar to a "matrix-valued" one-dimensional lattice. Due to this, it is natural to generalize the well-known recursive Green's function (RGF) [46–48] to this one-dimensional lattice in the Fock space. We define a *disconnected* Green's function matrix for a sector α_i by $[\mathcal{G}^0]^{-1}_{\alpha_i\alpha_i}(\omega) \equiv \omega - H(\alpha_i) + i\eta$. As mentioned above, $H(\alpha_i)$ represents H in the basis elements belonging only to the sector α_i. The dimension of $[\mathcal{G}^{0R(\mathcal{N})}]^{-1}_{\alpha_i\alpha_i}(\omega)$ and $H(\alpha_i)$ is ${}^{\mathcal{L}/2}C_{i-1} \times {}^{\mathcal{L}/2}C_{\mathcal{N}-i+1}$. This is because for the α_i sector, we have $n_l = i-1$ and $n_r = \mathcal{N} - n_l$. These matrices contain all interaction and hopping terms connecting the states that preserve the (n_l, n_r) pair. The NN sector connecting matrices, between adjacent α_i and $\alpha_i + 1$, denoted by $[\tau]_{\alpha_i,\alpha_{i+1}}$, has the dimension $({}^{\mathcal{L}/2}C_{\mathcal{N}-i+1} \times {}^{\mathcal{L}/2}C_i)$.

We also need to introduce an intermediate, *forward-connected* Green's function matrix, $[\mathcal{G}^F]_{\alpha_i\alpha_i}$, defined in Eq. (A5). Below we will show how to obtain retarded Green's function blocks $[\mathcal{G}^{\mathcal{N}}]_{\alpha_i\alpha_i}$, by a forward and backward recursion involving $[\mathcal{G}^F]_{\alpha_i\alpha_i}$, $[\mathcal{G}^0]^{-1}_{\alpha_i\alpha_i}$, and $[\tau]_{\alpha_i,\alpha_j}$. For notational brevity, we have suppressed the ω arguments. The recursive algorithm applied to the Fock-space lattice has the following steps:

(a) At first, the *forward-connected* Green's function is calculated by the recursive equation

$$[\mathcal{G}^F]^{-1}_{\alpha_i\alpha_i} = [\mathcal{G}^0]^{-1}_{\alpha_i\alpha_i} - [\tau]_{\alpha_i\alpha_{i-1}} [\mathcal{G}^F]_{\alpha_{i-1}\alpha_{i-1}} [\tau]_{\alpha_{i-1}\alpha_i}. \tag{A5}$$

For a system with periodic or open boundary conditions, we start with the α_1 sector, with $(n_l = 0, n_r = \mathcal{N})$. Since there is no block to its left, from the above equation, $[\mathcal{G}^F]_{\alpha_1\alpha_1} =$

$[\mathcal{G}^0]_{\alpha_1\alpha_1}$. Starting from this, we obtain all other diagonal blocks of the *forward-connected* Green's function up to $[\mathcal{G}^F]_{\alpha_{\mathcal{N}+1}\alpha_{\mathcal{N}+1}}$, which is the $\alpha^{th}_{\mathcal{N}+1}$ block. Since there are no further blocks, it can be shown that $[\mathcal{G}^F]_{\alpha_{\mathcal{N}+1}\alpha_{\mathcal{N}+1}} = [\mathcal{G}]_{\alpha_{\mathcal{N}+1}\alpha_{\mathcal{N}+1}}$, the retarded Green's function of the $\alpha_{\mathcal{N}+1}$ block [46].

(b) From $[\mathcal{G}]_{\alpha_{\mathcal{N}+1}\alpha_{\mathcal{N}+1}}$, all other diagonal blocks of the retarded Green's function can be obtained by a backward recursion equation,

$$[\mathcal{G}]_{\alpha_{i-1}\alpha_{i-1}} = [\mathcal{G}^F]_{\alpha_{i-1}\alpha_{i-1}}(I + [\tau]_{\alpha_{i-1}\alpha_i}[\mathcal{G}]_{\alpha_i\alpha_i}[\tau]_{\alpha_i\alpha_{i-1}}[\mathcal{G}^F]_{\alpha_{i-1}\alpha_{i-1}}).$$

(c) From the diagonal blocks of the retarded Green's function, we can calculate all off-diagonal blocks by the recursive relation

$$[\mathcal{G}]_{\alpha_i\alpha_j}|_{\alpha_i<\alpha_j} = -[\mathcal{G}^F]_{\alpha_i\alpha_i}[\tau]_{\alpha_i\alpha_{i+1}}[\mathcal{G}]_{\alpha_{i+1}\alpha_j}.$$

We note that matrix inversions are *only needed in the forward recursion*, and the largest matrix dimension that needs to be inverted is for the $\alpha_{\mathcal{N}/2}$ block. As seen from the above equations, we need two matrices of the dimension of the sector α_i, and α_i at the ith step of the recursion. Any matrix multiplication to obtain $[\tau]_{\alpha_i\alpha_{i-1}}[\mathcal{G}^F]_{\alpha_{i-1}\alpha_{i-1}}[\tau]_{\alpha_{i-1}\alpha_i}$ is calculated in a manner that the connection matrices and the relevant Green's function matrices are not simultaneously allocated in the memory. Finally, each frequency point is calculated independently, adding no significant memory overhead.

As detailed in our recent paper [37], due to these features, i.e., the requirements of F-RGF, the exponential growth of the Hilbert space is suppressed by $(1/\mathcal{L})$. This leads to the following major practical advantage. For, say, $N = 20$ and half filling, i.e., the current state of the art, this amounts to a reduction of RAM from 512 Gb to a mere 160 Gb. It shows that we can perform state-of-the-art calculations at a fractional memory at other fillings as well, allowing access to large system sizes with currently available resources.

3. Bandwidth of two-hole bound pair

We estimate the bandwidth of a two-hole bound pair by constructing an effective Hamiltonian by dividing the basis vectors into two groups: (i) all states with two holes on NN sites and (ii) all other states. We separately construct the Hamiltonian for these two groups, H_{2h} and H_r, respectively. The full Hamiltonian is a direct sum of these two apart from the connection terms between them. Thus, H is given by

$$H = \begin{bmatrix} H_{2h} & H_c \\ H_c & H_r \end{bmatrix}.$$

Here, H_c are the hopping terms that connect the states of H_{2h} and H_r. Using standard manipulations, we can write

$$H^{\text{eff}}_{2h}(\omega) = \omega - \left[(\omega - H_{2h}) - H_c\frac{1}{(\omega - H_r)}H_c\right]. \tag{A6}$$

We set $\omega = -3U$ as the potential energy of all states with two holes on NN sites to obtain the low-energy effective Hamiltonian. We note that this procedure is valid only if there is a clear energy separation between the states of H_{2h} and H_r. The bandwidth in the inset of Fig. 1 (dashed line) is the bandwidth of the spectrum obtained by diagonalizing $H^{\text{eff}}_{2h}(-3U)$. D_{BW} at large U can also be estimated analytically by the standard perturbation approach to the order of $O(t^2/U)$ and is found to be $4t^2/U$.

[1] K. Winkler, G. Thalhammer, F. Lang, R. Grimm, J. Hecker Denschlag, A. J. Daley, A. Kantian, H. P. Büchler, and P. Zoller, Nature (London) **441**, 853 (2006).

[2] F. J. Teran, L. Eaves, L. Mansouri, H. Buhmann, D. K. Maude, M. Potemski, M. Henini, and G. Hill, Phys. Rev. B **71**, 161309(R) (2005).

[3] V. Efimov, Phys. Lett. B **33**, 563 (1970).

[4] S. E. Pollack, D. Dries, and R. G. Hulet, Science **326**, 1683 (2009).

[5] F. Gel'mukhanov, M. Odelius, S. P. Polyutov, A. Föhlisch, and V. Kimberg, Rev. Mod. Phys. **93**, 035001 (2021).

[6] A. Trützschler, M. Huth, C.-T. Chiang, R. Kamrla, F. O. Schumann, J. Kirschner, and W. Widdra, Phys. Rev. Lett. **118**, 136401 (2017).

[7] R. Gotter, A. Verna, M. Sbroscia, R. Moroni, F. Bisio, S. Iacobucci, F. Offi, S. R. Vaidya, A. Ruocco, and G. Stefani, Phys. Rev. Lett. **125**, 067202 (2020).

[8] M. Ediger, G. Bester, A. Badolato, P. M. Petroff, K. Karrai, A. Zunger, and R. J. Warburton, Nat. Phys. **3**, 774 (2007).

[9] C. Verdozzi, M. Cini, and A. Marini, J. Electron Spectrosc. Relat. Phenom. **117-118**, 41 (2001).

[10] G. A. Sawatzky, Phys. Rev. Lett. **39**, 504 (1977).

[11] M. Cini, Solid State Commun. **24**, 681 (1977).

[12] E. Antonides, E. C. Janse, and G. A. Sawatzky, Phys. Rev. B **15**, 1669 (1977).

[13] D. E. Ramaker, Crit. Rev. Solid State Mater. Sci. **17**, 211 (1991).

[14] L. C. Davis, J. Appl. Phys. **59**, R25 (1986).

[15] J. Ghijsen, L. H. Tjeng, J. van Elp, H. Eskes, J. Westerink, G. A. Sawatzky, and M. T. Czyzyk, Phys. Rev. B **38**, 11322 (1988).

[16] E. V. n. Boström, M. Gisselbrecht, T. Brage, C.-O. Almbladh, A. Mikkelsen, and C. Verdozzi, Phys. Rev. Lett. **121**, 233201 (2018).

[17] X.-C. Huang, X.-J. Kong, T.-J. Li, Z.-R. Ma, H.-C. Wang, G.-C. Liu, Z.-S. Wang, W.-B. Li, and L.-F. Zhu, Phys. Rev. Res. **3**, 033063 (2021).

[18] E. P. Kanter, B. Krässig, Y. Li, A. M. March, P. Ho, N. Rohringer, R. Santra, S. H. Southworth, L. F. DiMauro, G. Doumy, C. A. Roedig, N. Berrah, L. Fang, M. Hoener, P. H. Bucksbaum, S. Ghimire, D. A. Reis, J. D. Bozek, C. Bostedt, M. Messerschmidt *et al.*, Phys. Rev. Lett. **107**, 233001 (2011).

[19] Y. Velkov, Y. Hikosaka, E. Shigemasa, T. Kaneyasu, Y. Tamenori, J.-C. Liu, and F. Gel'mukhanov, Phys. Rev. A **79**, 022508 (2009).

[20] N. Rohringer and R. Santra, Phys. Rev. A **77**, 053404 (2008).

[21] A. Kivimäki, A. Naves de Brito, S. Aksela, H. Aksela, O.-P. Sairanen, A. Ausmees, S. J. Osborne, L. B. Dantas, and S. Svensson, Phys. Rev. Lett. **71**, 4307 (1993).

[22] Z. F. Liu, G. M. Bancroft, K. H. Tan, and M. Schachter, Phys. Rev. Lett. **72**, 621 (1994).

[23] S. Aksela, E. Kukk, H. Aksela, and S. Svensson, Phys. Rev. Lett. **74**, 2917 (1995).
[24] E. Kukk, H. Aksela, S. Aksela, F. Gel'mukhanov, H. Ågren, and S. Svensson, Phys. Rev. Lett. **76**, 3100 (1996).
[25] O. Gunnarsson and K. Schönhammer, Phys. Rev. B **22**, 3710 (1980).
[26] M. Cini, Surf. Sci. **87**, 483 (1979).
[27] A. Marini and M. Cini, Phys. Rev. B **60**, 11391 (1999).
[28] M. Potthoff, J. Braun, and G. Borstel, Z. Phys. B **95**, 207 (1994).
[29] M. Potthoff, J. Braun, G. Borstel, and W. Nolting, J. Electron Spectrosc. Relat. Phenom. **72**, 163 (1995).
[30] D. D. Sarma and P. Mahadevan, Phys. Rev. Lett. **81**, 1658 (1998).
[31] H. Eskes and G. A. Sawatzky, Phys. Rev. B **44**, 9656 (1991).
[32] J. Zaanen, C. Westra, and G. A. Sawatzky, Phys. Rev. B **33**, 8060 (1986).
[33] O. Gunnarsson and K. Schönhammer, Phys. Rev. B **28**, 4315 (1983).
[34] A. Mukherjee, G. A. Sawatzky, and M. Berciu, Phys. Rev. B **87**, 165136 (2013).
[35] M. Möller, A. Mukherjee, C. P. J. Adolphs, D. J. J. Marchand, and M. Berciu, J. Phys. A: Math. Theor. **45**, 115206 (2012).
[36] J. Zaanen, G. A. Sawatzky, and J. W. Allen, Phys. Rev. Lett. **55**, 418 (1985).
[37] Prabhakar and A. Mukherjee, J. Phys. A: Math. Theor. **56**, 385204 (2023).
[38] M. Potthoff, J. Braun, G. Borstel, and W. Nolting, Phys. Rev. B **47**, 12480 (1993).
[39] F. Hofmann and M. Potthoff, Phys. Rev. B **85**, 205127 (2012).
[40] R. Rausch and M. Potthoff, New J. Phys. **18**, 023033 (2016).
[41] K. Wandelt, G. Mondio, and G. Cubiotti, in *Auger spectroscopy and electronic structure: Proceedings of the First International Workshop* (Springer Berlin, Heidelberg, 1988), Chap. 1.
[42] G. Greczynski and L. Hultman, Prog. Mater. Sci. **107**, 100591 (2020).
[43] T. Egami, S. Ishihara, and M. Tachiki, Science **261**, 1307 (1993).
[44] N. Nagaosa and J.-i. Takimoto, J. Phys. Soc. Jpn. **55**, 2735 (1986).
[45] G. Jana, A. Joshi, S. Pal, and A. Mukherjee, Commun. Phys. **5**, 66 (2022).
[46] D. J. Thouless and S. Kirkpatrick, J. Phys. C **14**, 235 (1981).
[47] P. Drouvelis, P. Schmelcher, and P. Bastian, J. Comput. Phys. **215**, 741 (2006).
[48] E. M. Godfrin, J. Phys.: Condens. Matter **3**, 7843 (1991).